



A long-term charge/discharge cycle at Mt. Etna volcano revealed through absolute gravity and GPS measurements

Filippo Greco¹ · Alessandro Bonforte¹ · Daniele Carbone¹

Received: 12 January 2022 / Accepted: 29 November 2022
© The Author(s) 2022

Abstract

We present results of repeated absolute gravity and GPS measurements, carried out at Mt. Etna volcano between 2009 and 2018. Absolute gravity measurements are rarely performed along arrays of stations on active volcanoes and, through our unprecedented dataset, we highlight the possibilities of this method to track underground mass changes over long time-scales. Analysis of the residual absolute gravity data and ground deformation reveals a cycle of gravity increase and uplift during 2009 to 2011, followed by gravity decrease and subsidence during 2011 to 2014. Data inversion points to a common mass and pressure source, lying beneath the summit area of the volcano, at depth of ~ 5 km b.s.l. The bulk volume change inferred by the inversion of the deformation data can account for only a small portion of the mass change needed to explain the correspondent gravity variations. We propose that the observed relationship between gravity and vertical deformation was mostly due to the compressibility of the magma in the inferred reservoir, which, in turn, was enhanced by the presence of exsolved gas. Overall, the gravity and deformation data we present reveal a cycle of magma recharge (2009–2011) and discharge (2011–2014) to/from the inferred storage zone. During the recharge phase only degassing occurred from the summit craters of Mt. Etna. During the following phase of discharge, the magma lost from the reservoir at ~ 5 km b.s.l. fed the exceptional phase of volcanic activity during 2011–2014, when tens of lava fountaining episodes took place.

Keywords Absolute gravity data · Ground deformation · Mount Etna · Charge/discharge cycle · Lava fountaining activity

1 Introduction

One of the key challenges of modern volcanology is to identify and characterize the ongoing state of activity of volcanoes, through recognition of meaningful changes in observable parameters. This helps to increase the efficiency of hazard mitigation plans, thus reducing the impact of eruptive events on the populations that live in the vicinity of active volcanoes. The joint use of different geophysical, geochemical and volcanological parameters allows to improve the possibilities of volcano monitoring, thus enhancing the quality of the models that are used to understand the driving processes of eruptive events (Acocella et al. 2016; Alparone et al. 2011; Bonaccorso et al. 2011a, b, c; Carbone et al. 2015; Hajian et al. 2019).

Volcanic unrest is often accompanied by surface deformation and gravity changes (Berrino et al. 1992; Battaglia et al. 2003; Bonforte et al. 2007, 2017; Greco et al. 2016; Carbone et al. 2017). Accordingly, high-precision gravity and ground deformation measurements are increasingly performed to monitor active and quiescent volcanoes. They allow discovery of magma transfers across the feeding systems of active volcanoes (Bonaccorso et al. 2011a; Del Negro et al. 2013), changes in the amount of exsolved volatiles in magma reservoirs (Carbone et al. 2015) and changes in the rate of fracturing of the hosting medium (Carbone et al. 2009, 2014; Greco et al. 2010). Gravity and ground deformation measurements complement each other, thus providing a more complete information on the processes driving the phases of unrest (Battaglia et al. 2008; Bonforte et al. 2007).

At Mt. Etna volcano (Italy), gravity and ground deformation measurements have been accomplished since the eighties, either individually or jointly (Budetta et al. 1989; Obrizzo et al. 2004; Puglisi et al. 2004; Bonaccorso et al. 2011a; Alparone et al. 2013), allowing to shed light on the volcanic processes in the shallow and intermediate plumbing

✉ Filippo Greco
filippo.greco@ingv.it

¹ Istituto Nazionale di Geofisica e Vulcanologia - Sezione di Catania - Osservatorio Etneo, Catania, Italy

system of the volcano (Bonforte et al. 2007; 2017; Carbone and Greco 2007; Carbone et al. 2015; Del Negro et al. 2013; Greco et al. 2016).

Gravity changes associated with volcanic processes occur over a wide range of time scales, from minutes to years and with magnitude between a few and a few hundred μGal ($1 \mu\text{Gal} = 10^{-8} \text{ms}^{-2}$). High-precision instruments are necessary to detect such small signals and both time-lapse surveys, along networks of stations, and continuous measurements, at single points, are carried out. Time lapse surveys can be carried out with relative (spring) gravimeters, that measure gravity differences over space, between pairs of stations, or by absolute gravimeters, capable of measuring the actual value of the gravitational acceleration at the observation point (Carbone et al. 2017; Greco et al. 2012).

In order to accurately measure small gravity changes due to volcanic processes (few μGal), repeated absolute gravity (AG) measurements have been performed at Mt. Etna (Italy) using the IMGC-02 (D'Agostino et al. 2008) and the Microg LaCoste FG5#238 gravimeters, since 2007 and 2009, respectively (Pistorio et al. 2011; Greco et al. 2012, 2015). Even though the use of absolute gravimeters on active volcanoes implies many difficulties (e.g. transport of the instrumentation, power supply at sites where mains electricity is not available), AG measurements may successfully replace or supplement relative gravity surveys, which often require a significant effort to mitigate the effect of instrumental drift and tares (Rymer 1989). The availability of absolute measurements in points very close to active volcanic structures provides accurate information on the changes related to magmatic processes.

At Mt. Etna, ground deformation measurements were first performed using the Electronic Distance Measurement (EDM) technique (Puglisi et al. 2004; Alparone et al. 2013) that has been later replaced by Global Positioning System (GPS), gradually evolved to Global Navigation Satellite Systems (GNSS). While EDM measurements were able to provide changes in the distances between pairs of points, GPS measurements provide the 3D position of a point on the surface. Continuous GPS measurements are carried out at Mt. Etna across a network that includes about 40 stations (Bruno et al. 2012). Time lapse surveys are also accomplished (at least once per year) to obtain a more detailed picture of the ground deformation pattern on a denser network, including several benchmarks in the most active areas.

Even considering the long history of gravity measurements at Mt Etna, a 10-year-long dataset of absolute gravity measurements, collected at one of the most active volcanoes in the world, is unprecedented and in itself exceptional, especially if one considers that: (i) high-quality measurements were collected by moving and installing absolute gravimeters, engineered for quiet laboratory conditions, in the harsh

environments that characterize the summit zone of the volcano; (ii) the data allow to coherently track also small gravity changes occurring over time scales of years. Furthermore, through comparison with correlated ground deformation data, we reveal a mechanism of long-term magma accumulation and discharge, involving a strong “mass excess”.

Here, we present the results obtained through the joint analysis of repeated AG and GPS measurements at Mt. Etna over a 10-year-long interval, during which the volcano displayed a lively eruptive activity, with several lava fountain events and intense Strombolian activity from the summit craters. We demonstrate that the joint study of gravity and GPS data is crucial for better understanding the driving volcanic processes, drawing conclusions behind the volcanic activity, which couldn't be reached if only one of the two dataset was available.

2 Review of Mt. Etna activity during 2009 to 2018

After the 2008–2009 flank eruption (Napoli et al. 2008), Mt. Etna (Fig. 1a) remained largely quiescent until 2010. Explosive activity resumed on 11 January 2011 from a pit on the east flank of the South-East Crater (SEC), one of the four summit craters of Mt. Etna (Fig. 1b). Between January 2011 and December 2013, 44 lava fountaining episodes (Fig. 1c) occurred from this vent (Calvari et al. 2018). Among these, only 4 episodes took place during the first half of 2011, while, since July, 13 events occurred in slightly more than 100 days (early July to late October 2011). Other clusters of closely spaced events occurred between early March and late May 2012 (5 events in 75 days), between mid-February and late April 2013 (13 events in less than 70 days; Cannata et al. 2015; Spampinato et al. 2015; Bruno et al. 2016), between late October and early December 2013 (6 events in less than 40 days). Between the two phases of closely spaced lava fountains in 2012 and early 2013, mild and intermittent eruptive activity occurred from the Bocca Nuova (BN) summit crater (Fig. 1b), between July and October 2012. As a consequence of this activity, a cinder cone and a lava flow field formed within the Bocca Nuova crater (Cannata et al. 2015; Slatcher et al. 2015; Spampinato et al. 2015). It is worth noting that, during the lava fountain on 26 October 2013, another summit crater (the North-East Crater (NEC); Fig. 1b) erupted simultaneously with the SEC (Fig. 1d).

The accumulation of the ballistics emitted during the 44 lava fountaining episodes led to the formation of a new cinder cone (the NSEC), which grew on the east flank of the SEC. After the 2011–2013 NSEC lava fountains, the eruptive activity switched to moderate lava effusion from the NSEC, during January–April and July–August 2014. On 28 Decem-

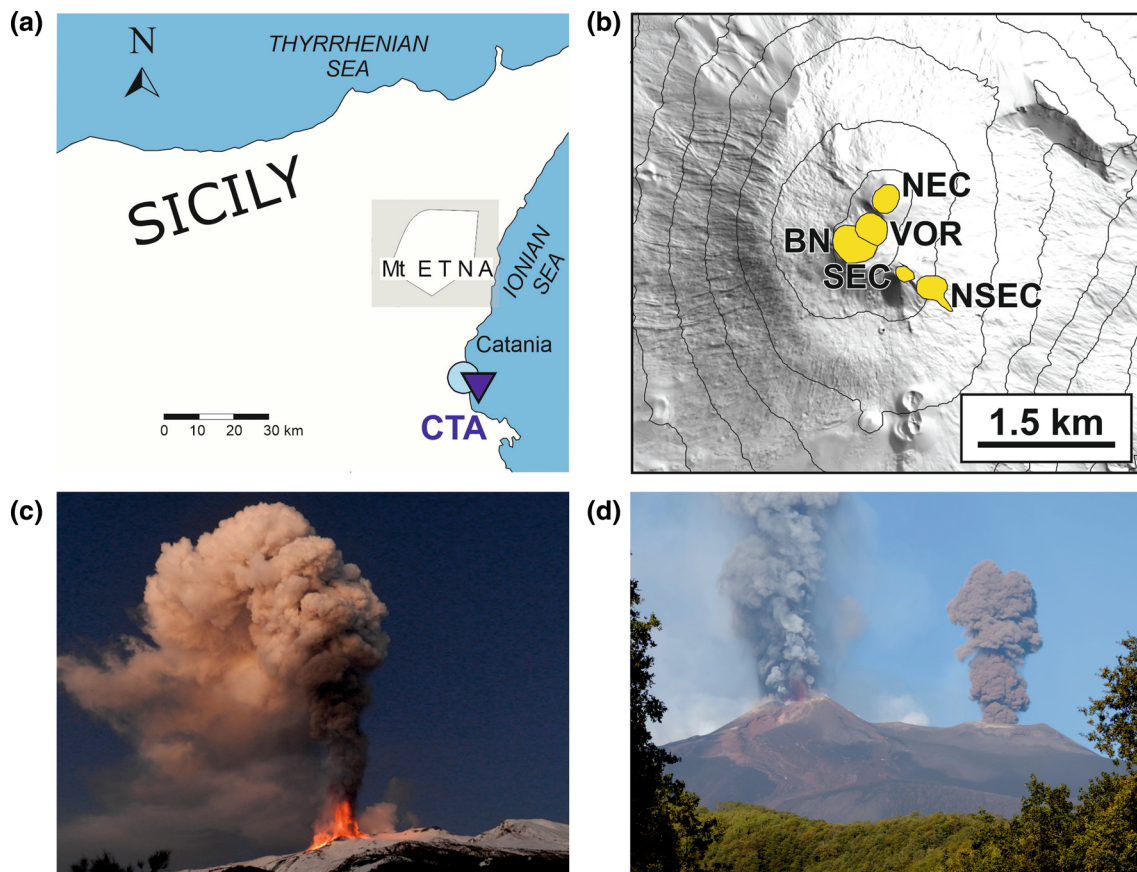


Fig. 1 **a** sketch map of the eastern side of Sicily showing the position of Mt. Etna and the CTA absolute gravity station, in the town of Catania, which is used as reference; **b** the active craters in the summit zone of Mt. Etna (VOR, Voragine; BN, Bocca Nuova; NEC, North-East Crater; SEC, South-East Crater; NSEC, New South-East Crater); **c** the January

5, 2012 eruption, one of the numerous lava fountaining episodes from the NSEC of Mt. Etna; **d** twin volcanic plumes on October 26, 2013 from NSEC (on the left of the photo) and from SEC (on the right of the photo). Photos **(c)** and **(d)**: credit by Boris Behncke, INGV—Osservatorio Etneo

ber 2014, a further lava fountain episode occurred from the NSEC, bringing the number of events to 45 (Bonforte and Guglielmino 2015).

During 2011–2014, a total volume of $\sim 150 \times 10^6 \text{ m}^3$ (pyroclastics products plus lava flows) erupted from the NSEC through lava fountain episodes (De Beni et al. 2015). Due to the high frequency of explosive episodes, the average eruption rate in this period is close to the rate observed during longer-term major effusive eruptions (Aloisi et al. 2018).

In January 2015, ash plume emissions started from the Voragine crater (VOR). Explosive activity from this crater increased in intensity and became almost regular since 27 October. It climaxed with two sequences of 4 and 3 events from the Voragine crater (VOR) on 3–5 December 2015 (Vulpiani et al. 2016) and on 18–21 May 2016, respectively, bringing to a total of 52 the episodes of lava fountaining from Mt. Etna's summit craters during January 2011 to May 2016. The lava fountains of 3–5 December 2015 rank among the most violent that have occurred at Mt. Etna in the last two

decades (Aloisi et al. 2017; Bonaccorso and Calvari 2017). After the major explosive events in May 2016, volcanic activity subsided for a few months. Strombolian eruptions and lava flows took place at the end of January 2017 and the activity intensified at the end of February 2017, with several lava flows issued from a new vent in the saddle between NSEC and SEC, until the end of April 2017. During June 2017–August 2018, fumarolic activity persisted at several locations in the crater area, and, on a few occasions, minor ash emissions were observed.

3 Mt. Etna's gravity and geodetic monitoring networks

A network for relative gravity measurements has been operated at Mt. Etna since 1986 (Budetta et al. 1989, 1999). The network has evolved over the years and it currently consists of 71 benchmarks, covering an area of about 400 km^2 . LaCoste

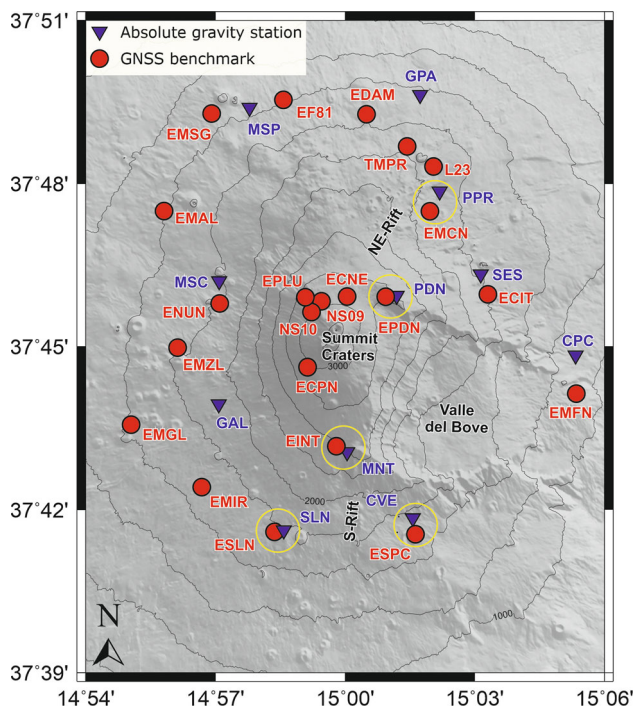


Fig. 2 Sketch map of Mt. Etna showing the positions of the stations for absolute gravity measurements (blue triangles) and the benchmarks for GPS measurements (red circles). The yellow circles highlight the absolute gravity stations and GPS benchmarks whose data are shown in Fig. 4

and Romberg model D and Scintrex CG-3 M/CG-5 gravimeters have been utilized to perform the relative measurements (Budetta and Carbone 1998; Carbone et al. 2009; Greco et al. 2014).

To achieve a balance between quality and efficiency in gravity measurements, we have investigated the applicability of absolute gravity measurements for volcano monitoring purposes. The first 4 stations for absolute measurements at Mt. Etna were installed in 2007, along a North–South profile crossing the summit craters, at elevations between about 1700 and 2850 m a.s.l. (SLN, MNT, PPN and PPR; Fig. 2). Another station was installed far from the summit active craters, in the facilities of INGV–OE (town of Catania, 50 m a.s.l.; CTA in Fig. 1a), intended as primary reference station. In 2009, we added 7 more stations (GAL, MSC, MSP, GPA, SES, CPC, CVE; Fig. 2), arranged as a ring around the volcano at elevations between 1150 and 2000 m a.s.l. (Greco et al. 2012, 2015).

Currently, the network for AG measurements includes, besides CTA, 11 stations, evenly distributed around the volcano edifice (Fig. 2). An absolute gravity station consists of a facility with a proper installation surface and providing protection to the instrumentation against ambient factors. Indeed, the main constraint when defining the position of a new absolute gravity station on Mt. Etna is the presence of

a facility to house the instrumentation. Even though absolute measurements are time-consuming (with a FG5, each measurement requires about 8–10 h to complete), the data quality is significantly improved with respect to the use of spring-type gravimeters. In order to check the performance of the absolute gravimeter, we conducted repeated measurements at CTA station (mostly at the beginning and at the end of each survey at Mt. Etna), where FG5#238 is usually maintained. We obtained a good reproducibility of the absolute measurements at this station, with uncertainties on each measurement ranging between 2.5 and 7.8 μGal . The standard deviation of 31 measurements, carried out during 2009 to 2018, is 3.2 μGal (Fig. 3). FG5#238 is also routinely checked against other absolute gravimeters, in the framework of international and regional inter-comparisons. The results provided by FG5#238 were consistent with the Key Comparison Values (Jiang et al. 2012; Greco et al. 2015; Newell et al. 2017; Pálinkáš et al. 2017; Falk et al. 2020). Absolute gravimeters are compared for the purpose of assuring their reliability and ensure the traceability of measurements to the SI units. On the other hand, comparisons are also essential for long-term absolute measurements in geodesy and geophysics to insure the consistency of the observations over a time period of decades.

The whole Mt. Etna's gravity network is occupied every summer. More frequent measurements are carried out through relative spring gravimeters across same elements of the network (almost monthly along an East–West profile; Carbone et al. 2009; Greco et al. 2010; Del Negro et al. 2013; Bonforte et al. 2017), or during eruptive events.

Ground deformation monitoring of Mt. Etna started in the 70's and has evolved ever since, in both networks and methods. Upgrades to the GPS network for repeated measurements have been accomplished also considering the opportunity of having the benchmarks in the same position as (or within close distance from) those used to perform gravity and other geophysical measurements (Puglisi et al. 2004). Most of the gravity and GPS benchmarks are co-located or within a few meters (Bonforte et al. 2007), with the exception of some sites where the distance is of the order of a few hundred meters. The whole GPS network (about 80 benchmarks) is surveyed at least once every year. Here, we present data from 22 GPS benchmarks (Fig. 2), of which 11 are co-located with absolute gravity stations, 5 lie on the summit area and 6 are located on sites not or slightly affected by the east flank seaward sliding (Bonforte et al. 2011). Measurements are usually performed during the summer, when, due to the lack of snow cover, the summit stations can be reached. Data are analysed jointly with data from the 40 continuously running GPS stations, in order to obtain information about the changes during the period between two subsequent campaigns at a higher space resolution (Bonforte et al. 2008). Additional surveys may also be carried out along parts of the

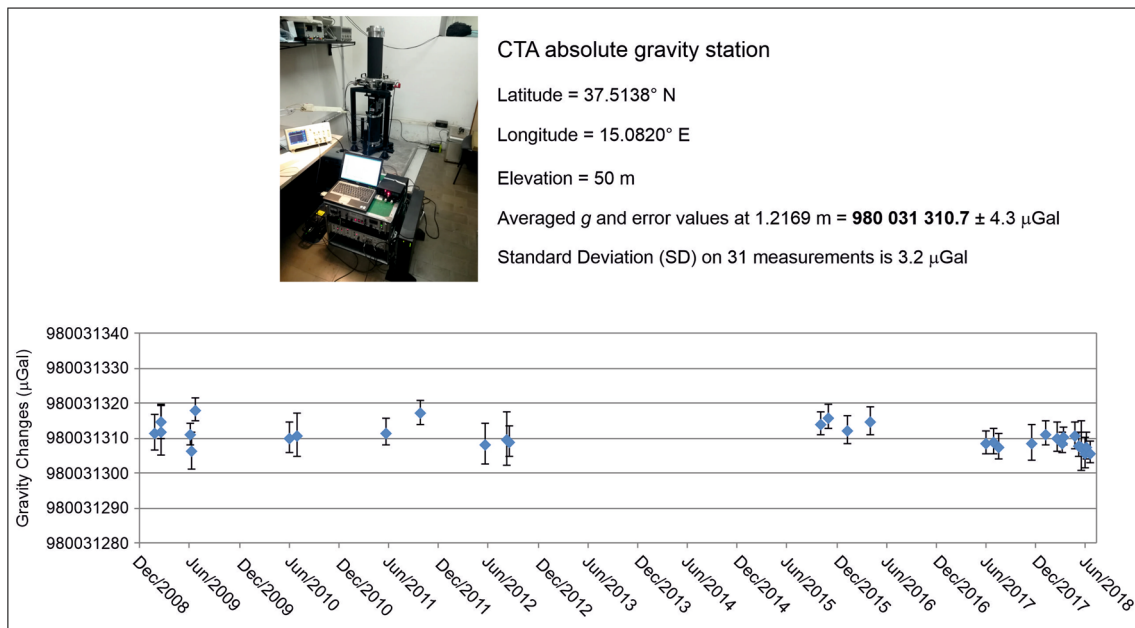


Fig. 3 Top: The FG5#238 absolute gravimeter during a measurement session at CTA station in the town of Catania (see Fig. 1a for the location of CTA station). The coordinates of the station, its elevation, the averaged value of g during the 2009–2018 interval, the combined averaged uncertainty ($\pm 4.3 \mu\text{Gal}$) and the standard deviation of 31 measurements ($3.2 \mu\text{Gal}$) are also reported. Bottom: Absolute gravity values

at CTA (Catania) station during 2009–2018 period, collected with the Micro-g LaCoste FG5#238 absolute gravimeter. The values of g are referred to an elevation of 1.2169 m from the ground, corresponding to the distance between the ground and the effective position of free-fall for FG5#238. The error bars represent the combined uncertainty

periodic network, during eruptive or seismic crises, in order to improve the time resolution of the data (Bonforte et al. 2013, 2017). On rare occasions, GPS measurements could not be performed at sites where absolute gravity measurements were carried out (e.g. due to the dense vegetation that masks the GPS satellite signal). In these cases, the information on ground deformation was retrieved using data from the other closer GPS benchmarks.

4 Repeated absolute gravity and GPS measurements

Between 2009 and 2018, we conducted almost yearly AG campaigns at Mt. Etna, using the FG5#238 free-fall gravimeter. In addition to AG measurements, vertical gravity gradient (VGG) measurements were performed using a spring relative instrument. More frequent AG measurements were carried out at SLN, CVE and CTA stations (Fig. 2). At SLN and CVE almost monthly relative gravity data were also collected through a spring gravimeter, which were employed to improve the time resolution of the changes observed through AG measurements. The averaged combined uncertainty estimated for all the gravity measurements is $7.1 \mu\text{Gal}$.

The gravity changes likely due to volcanic processes are obtained after correcting the data for effects of Earth tides

and polar motion, in compliance with the International Earth Rotation and Reference Systems Service (IERS) conventions 2010 (Petit and Luzum, 2010). The effect of atmospheric mass variations is also removed using the standard barometric admittance factor of $-0.3 \mu\text{Gal/hPa}$ (Merriam, 1992).

Usually, absolute gravity measurements are referred to a specific height above the station (from the ground) that mainly depends on the gravimeter type. Converting a measure taken at the real instrumental height into the corresponding value at any other height above the station needs accurate determination of the VGG. Since we used gravity data collected with both relative and absolute gravimeters, thus at different heights from the ground, to compare them, we used the local VGGs, measured using Scintrex relative gravimeters, to refer the relative gravity measurements to the common height of 1.2169 m (corresponding to the effective distance between the ground and the effective position of free-fall for FG5; Niebauer et al. 1995; Timmen 2003).

GPS measurements are conducted using multi-frequency GPS receivers in static mode on self-centring benchmarks. The latter is designed to eliminate setup errors and allow the maximum accuracy and repeatability of the measurements (Bonforte et al. 2016). The software used for processing GPS data is the last available version of a commercial survey data processing provided by Trimble® (Trimble Business Center). The overall procedure is the same used for

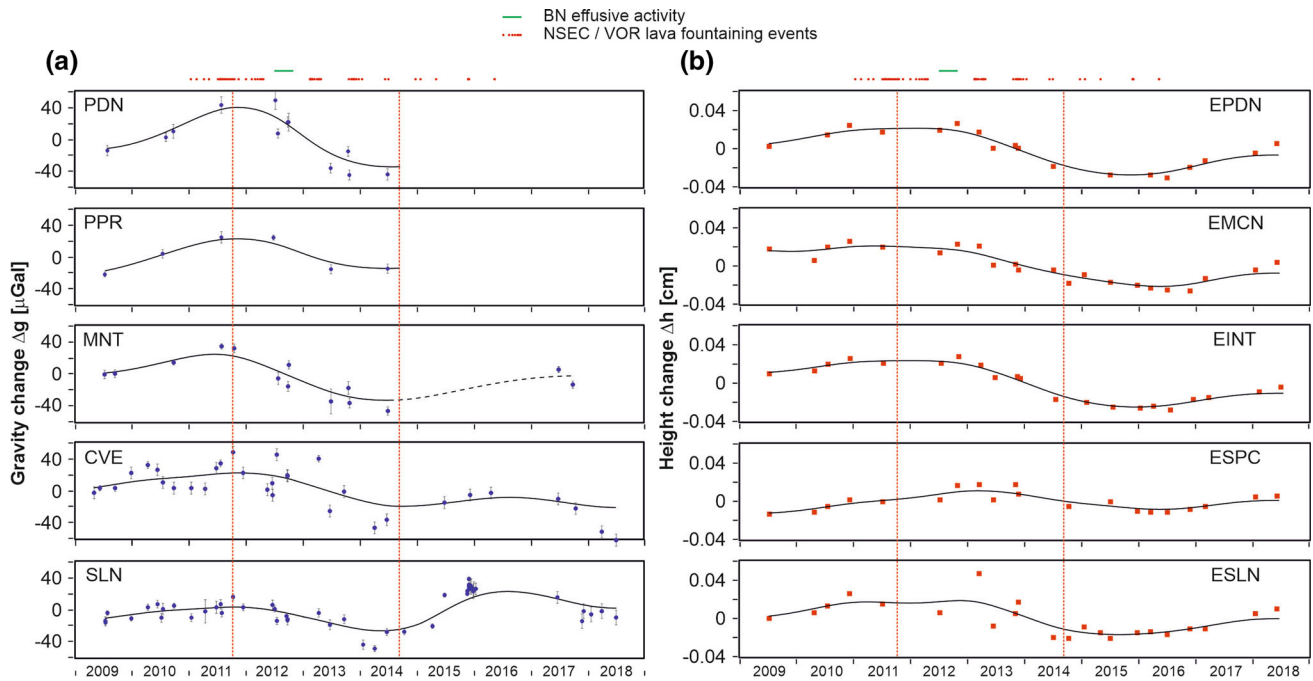


Fig. 4 Left: absolute gravity time series from five key stations of the network (marked with yellow circles in Fig. 2); the error bars indicate the combined uncertainty. Right: elevation time series from the five GPS benchmarks closest to the above key gravity stations. The black curves are low-pass filters, with cut-off period of about 3 years, applied to the

time series. The vertical red dashed lines mark the Nov-2011–Oct-2014 interval, which was selected for data modelling (see Sect. 6). On top of both sides of the figure, the red points and the green bar mark phases of eruptive activity

geodetic surveys on Sicilian volcanoes (Bonforte and Puglisi 2006; Bonforte and Guglielmino, 2008). GPS data are post-processed by using precise final ephemerides and precise antenna calibration models provided by IGS (Bonforte et al. 2013). To obtain the precise positioning of each GPS station, more than 20,000 baselines are usually processed when measuring the whole network and final solutions show 2–3 mm errors for the horizontal components and 3–4 mm for the vertical ones.

Both gravity and geodetic surveys were carried out in the same season of the year (late-spring to early-summer), thus minimizing seasonal effects due to the different water content in the subsoil.

5 Absolute gravity and elevation changes during the 2009–2018 period

AG values are corrected for local changes in elevation through the corresponding GPS data, using the experimental vertical gradient of gravity measured at each absolute station. Height-corrected absolute gravity time-series from five key stations of the network (Fig. 2) are presented in the left side of Fig. 4, while the corresponding elevation time-series from

the GPS benchmarks closest to the five gravity stations are shown in the right side of the same figure.

Both gravity and elevation time series show an increase/decrease cycle throughout 2009 to 2014 (Fig. 4a). In particular, a phase of gravity increase and uplift occurred between 2009 and late 2011, followed by a phase of gravity decrease and subsidence, between late 2011 and late 2014. This cycle affects the whole volcano edifice, with stronger variations mostly observed at the station closer to the summit craters (e.g. PDN and EPDN in Fig. 4).

To better evidence the increase/decrease cycle throughout the gravity and elevation data, we low-pass filter (cut-off period of 3 years) the time series from all available stations, after linear interpolation is applied to oversample the data at constant rate (1 day). The filtered time series are shown as black curves in Fig. 4. As for gravity, the increase and decrease phases reach a maximum amplitude (about +50 and -70 μGal , respectively) at PDN station (Fig. 4). Besides being stronger, the 2011–2014 decrease phase displays a more coherent pattern over space than the previous increase phase, as evidenced in Fig. 5. The patterns of the inflation and deflation phases during 2009 to 2014 have similar characteristics, even though the filtered amplitudes of the elevation changes during the inflation phase are more evenly distributed than the amplitudes of the corresponding gravity changes (Fig. 5).

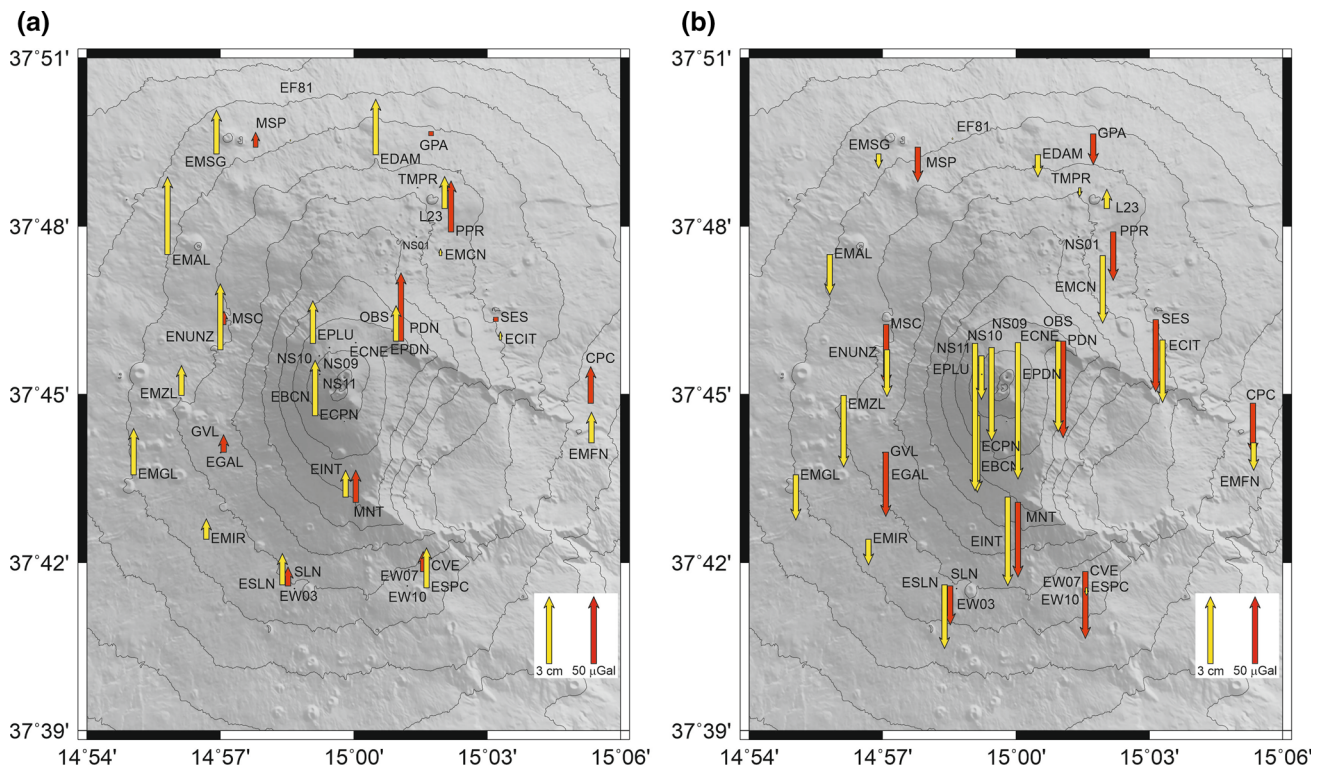


Fig. 5 Absolute height-corrected gravity changes (red arrows) and vertical deformation (yellow arrows) observed during 2009 to 2011 (a) and 2011 to 2014 (b). All changes are obtained using the low-pass filtered time series (cut-off period of about 3 years) from each observation point

During the subsidence phase, a maximum filtered amplitude of about -6 cm is reached at the stations closest to the summit craters (Fig. 5b).

After 2014, absolute gravity data were collected only at a few stations of the network and that explains why the three upper time-series in the left side of Fig. 4 provide information relevant only to the 2009–2014 interval. Hence, while the 2009–2014 cycle is well described by the available gravity data, from 2015 onwards, the available AG measurements do not allow to describe the gravity changes with adequate space and time resolution. The general pattern of the gravity changes during 2015 to 2018 can be retrieved using the data acquired at Serra La Nave (SLN) and Casa del Vescovo (CVE) stations, where almost yearly AG and ground deformation data were integrated with more frequent relative gravity measurements (Fig. 4). However, only qualitative inferences can be made on the data from only two stations, that could also reflect local effects, rather than being representative of the behaviour of the entire volcano.

6 Gravity and elevation changes during 2011 to 2014: data modelling

The fact that during 2009–2014 the residual gravity changes (i.e. after correction for the free air effect) share the same

increase/decrease pattern of vertical ground deformation (Fig. 4) indicates that the contribution to the observed gravity changes from the underground mass redistributions exceed the contribution due to the vertical displacement of the observation points (Battaglia et al. 2008).

To gain insight into the bulk mass and volume changes over the studied interval, we model gravity variation and deformation using analytical solutions. As reported in the previous section and shown in Fig. 5, the 2011–2014 phase of deflation and gravity decrease is characterized by slightly stronger amplitudes and more coherent patterns over space than the previous phase of uplift and gravity increase (2009–2011). Accordingly, to infer the characteristics of the pressure and mass sources, we invert deformation and residual gravity changes during 2011–2014. Given the similarity, in terms of time development, spatial pattern and amplitude of the changes between the phases of uplift/gravity increase and deflation/gravity decrease, we assume that the processes driving the observed changes during the whole considered interval (2009–2014) developed within the same source volumes and that similar mass and volume changes were involved during the two sub-intervals, with opposite sign.

Deformation and residual gravity changes are inverted separately, to produce independent models and avoid possible bias from forcing the solutions to share the same position.

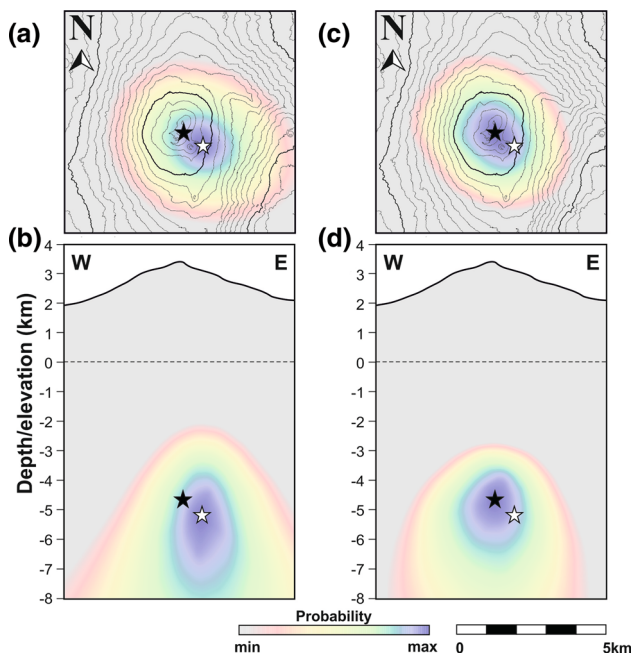


Fig. 6 (a) and (b) Mass source location probability on the horizontal and vertical (E-W trending) planes cutting the best-fit position (white star). At each node of the search grid, the location probability is obtained as the inverse of the sum of absolute deviations between observed and calculated gravity changes (see text). The black star marks the projection, on the same planes, of the best-fitting pressure source. (c) and (d) Pressure source location probability on the horizontal and vertical (E-W trending) planes cutting the best-fit position (black star). At each node of the search grid, the location probability is obtained as the inverse of the sum of absolute deviations between observed and calculated vertical deformations (see text). The white star marks the projection, on the same planes, of the best-fitting mass source

Residual gravity changes are inverted to constrain the source location and associated mass change. The low-pass filtered time-series of residual gravity changes (Fig. 5) from the 11 available absolute stations are used to evaluate the

changes during 2011–2014. As a forward model, we consider the gravitational attraction of a spherical body of finite size and mass, which is identical to that of a point source with the same mass (Battaglia and Hill, 2009). The spherical shape involves the minimum number of model parameters and was utilized not to over-interpret the relatively sparse available data. The best fit to the measured gravity changes is calculated through performing a minimization of the sum of absolute deviations (SAD), with respect to the involved parameters (location of the source model and mass change). To avoid possible convergence on local minima, the optimum solution is uniformly searched in a $6.5 \times 6.5 \times 6.5 \text{ km}^3$ volume around and beneath the summit craters. Results are shown in Fig. 6, as the location probability density (obtained from the inverse of the SAD values) within the search domain. The optimum mass-source model is centred slightly east of the summit craters (white star in Fig. 6a), at a depth of about 5 km b.s.l. (Fig. 6b). The mass decrease during 2011–2014 is modelled as $-7 \times 10^{11} \text{ kg}$ and the RMS error between observed and calculated (best-fit) gravity changes is $5 \mu\text{Gal}$ (Fig. 7).

The source of ground deformation is constrained through inversion of the vertical component of the GPS observations. The reason for disregarding the horizontal components of the deformation is that, over time-scales of years, they are dominated by the gravitational spreading of Mt. Etna's volcano edifice (Urlaub et al. 2018). This is shown by Aloisi et al. (2018), who analysed surface area changes recorded at intermediate altitude on the west flank of Mt. Etna, during 2009–2017. They showed that, even though areal dilatation/contraction cycles occur over time scales of months, there is a general dilatation trend, leading to an area increase of about 30 ppm, across the whole considered interval.

The low-pass filtered vertical deformation time-series from 22 GPS stations (Fig. 5) are used to create the database of changes during 2011–2014, which then become the input

Fig. 7 Observed and calculated gravity changes versus horizontal distance from the source. The RMS error between observed and calculated (best-fit) gravity changes is $5 \mu\text{Gal}$

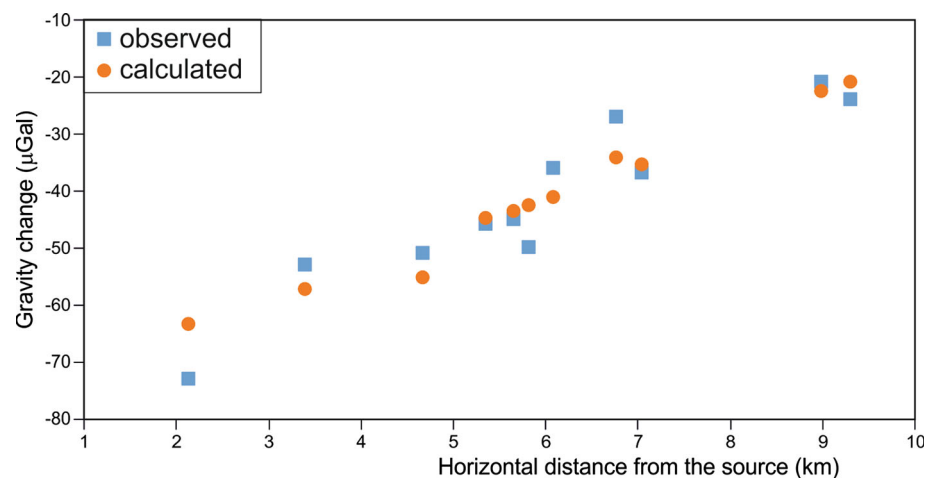
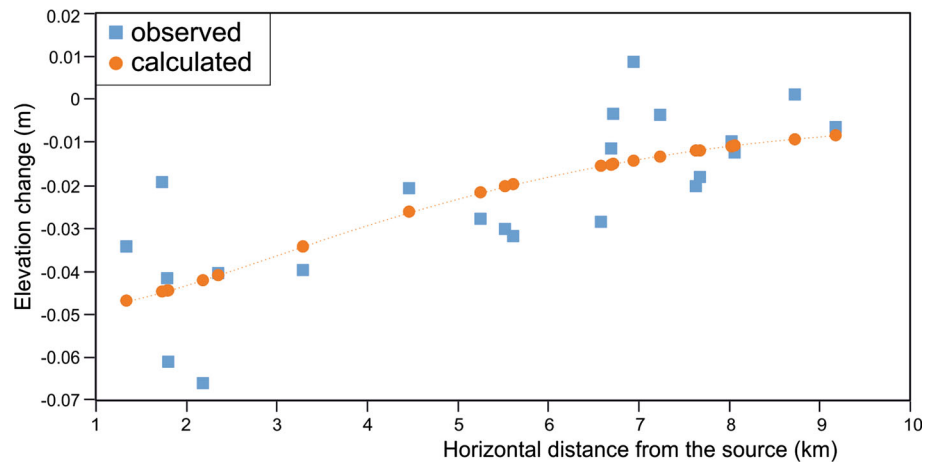


Fig. 8 Observed and calculated elevation changes versus horizontal distance from the source. The RMS error between observed and calculated (best-fit) elevation changes is 1.2 cm



to the inversion scheme. The latter involves a finite spherical magma body as the forward model of the pressure source, which is described through the analytical solution of McTigue (1987). Also in this case, the optimum solution is achieved through minimizing the SADs, while the source location probability is defined in the whole search domain (Panels c and d of Fig. 6). The optimum pressure-source model lies beneath the summit craters, at a depth of about 4700 m (black star in Fig. 6). The best solution involves a bulk volume decrease of $8 \cdot 10^6 \text{ m}^3$. The RMS error between observed and calculated (best-fit) elevation changes is 1.2 cm (Fig. 8).

A comparison between the results obtained through the inversion of the gravity and deformation data shows that the mass and pressure sources occupy similar positions. In particular, the location probability maps show that each source is placed in a position where the probability of finding the other one is high (Fig. 6). This observation implies that the deformation and gravity changes during the studied period are, most likely, different effects of the same overall source processes.

7 Gravity and elevation changes during 2015 to 2018

After the cycle of gravity increase and uplift, followed by gravity decrease and subsidence, during the interval between 2009 and 2014, a new phase of moderate uplift started in early 2016 and continued throughout 2018 (Fig. 4). Weak positive elevation changes (mostly less than 2 cm) were observed at most stations, but without a clearly defined spatial pattern.

After 2014, absolute gravity measurements were performed only at SLN and CVE stations (see Sect. 5 and Fig. 4). Data from the two stations highlight a relatively fast gravity increase (late 2014 to early-2016), which reached an amplitude of about $50 \mu\text{Gal}$ at SLN (Fig. 4), followed by an overall

gravity decrease until the end of the period considered in the present study.

Within the limits of the available data, we can conclude that the coupled behaviour of gravity and elevation changes which characterized the 2009–2014 interval did not continue after 2014. This could indicate a different behaviour of the volcano, which is indeed reflected in the different eruptive styles characterizing the years before and after early 2015.

8 Discussion

Residual absolute gravity measurements between 2009 and late 2014 highlight a cycle of gravity increase (2009–2011) and decrease (2011–2014), accompanied by synchronous ground elevation changes following the same pattern of increase (uplift) and decrease (subsidence; see Fig. 4). Inversion of residual gravity and deformation data during the 2011–2014 decrease phase indicates that, overall, the mass and pressure sources share a similar position beneath the summit area of the volcano, at a depth of $\sim 5 \text{ km}$ b.s.l. (Fig. 6). This suggests that, within the measurement and model uncertainty, the observed gravity changes and deformation are triggered by processes occurring in the same source volume. The latter is a well-known storage zone at intermediate depth (e.g. Bonforte et al. 2008; Aloisi et al. 2018). Nevertheless, while the inversion of vertical deformation points to a bulk volume decrease of $8 \cdot 10^6 \text{ m}^3$, a conservative estimate of the volume change from residual gravity variations is $250 \cdot 10^6 \text{ m}^3$, assuming a magma density of 2700 kg m^{-3} . Hence, even though the sources of deformation and gravity changes roughly coincide, the volume change inferred from the deformation is only 3% of the volume change inferred from residual gravity variations.

This kind of discrepancy was found at other volcanoes, like Piton de la Fournaise (La Réunion; Bonvalot et al. 2008), Askja and Krafla (Iceland; de Zeeuw-van Dalftsen

et al. 2005, 2006) and Kīlauea (Hawaii, Johnson et al. 2010). Residual gravity changes measured between 2009 and 2012 inside Kīlauea Caldera were accompanied by surface displacements of the same area. Modelling results indicated that the sources of deformation and gravity changes coincided, but the volume change inferred from deformation was only 8–9% of the volume changes inferred from residual gravity variations. Bagnardi et al. (2014) reviewed different processes able to produce bulk mass change without the expected corresponding volume change. Those include compression/decompression of the magma in the reservoir, substitution of the resident magma with magma having different density, and filling/emptying of void space.

Residual gravity changes pointing to the involvement of bulk volumes larger than expected from the associated ground deformation were observed at Mt. Etna on different occasions (e.g. Budetta et al. 1999; Carbone et al. 2003, 2008; Greco et al. 2016) and they were explained through mechanisms similar to those proposed by Bagnardi et al. (2014).

Currenti (2014) reviewed observations from Mt. Etna during September 1994 to October 1995 (Budetta et al. 1999) as a case study to show, through finite element modelling, that the source geometry may also play a significant role in controlling the relationship between gravity changes and ground deformation occurring at volcanoes. In particular, for ellipsoidal sources, the ratio of gravity change to vertical deformation may be higher than predicted by the Mogi model, leading to the possible development of major gravity changes without significant deformation. However, this is especially true in the case of relatively shallow sources.

According to Bonafede and Ferrari (2009), the magma stored in a reservoir (assumed spherical) can undergo a volume contraction/expansion (ΔV_{in}) equal to:

$$\Delta V_{in} = V_0 \Delta p \beta_m, \quad (1)$$

where V_0 is total volume of the reservoir, Δp is the pressure change and β_m is the compressibility of the resident magma. It also holds that the outwards volume expansion/contraction of the reservoir (ΔV_{out}) is (Bonafede and Ferrari, 2009):

$$\Delta V_{out} = V_0 \Delta p \frac{3}{4\mu}, \quad (2)$$

where μ is the rigidity modulus of the host medium. The overall volume change (ΔV_m), occurring when new magma is injected to or withdrawn from the reservoir, is (Bonafede and Ferrari 2009):

$$\Delta V_m = \Delta V_{out} + \Delta V_{in} = \Delta V_{out} \left(1 + \frac{4\mu\beta_m}{3} \right), \quad (3)$$

Our results point to a value of the ratio between ΔV_m (volume deduced from residual gravity) and ΔV_{out} (volume

deduced from ground deformation) on the order of 30, implying that:

$$1 + \frac{4\mu\beta_m}{3} \approx 30; \beta_m \approx \frac{22}{\mu} \quad (4)$$

Assuming a standard value for μ of 25 GPa and assuming that the observed $\Delta V_m / \Delta V_{out}$ ratio is due solely to shrinking of the magma inside the reservoir, from [4] we obtain $\beta_m \approx 0.9 \text{ GPa}^{-1}$. Compressibility of degassed basalts at crustal depths is in the range 0.06–0.1 GPa^{-1} (Rivalta and Segall, 2008), thus, about an order of magnitude lower than the above result. However, β_m can reach higher values (up to 3 GPa^{-1}), in the case of volatile-rich magmas stored at depths of > 3 km (Kilbride et al. 2016). Indeed, at Mt. Etna, CO_2 is thought to become exsolved at considerable depth ($p > 200 \text{ MPa}$; Moretti et al. 2018), implying that there could be a significant amount of volatiles in the magma reservoir at the inferred source depth of ~ 5 km.

Magma compressibility could thus explain, at least in part, the discrepancy between magma volumes deduced from gravity and ground deformation data.

Filling/emptying of void space by magma was also invoked to explain the occurrence of gravity changes with minor deformation at Mt. Etna (Rymer et al. 1993) and other volcanoes (e.g. Johnson et al. 2010). However, due to the increasing confining pressure, it is unlikely that open space may persist at depths of more than a few km beneath the surface, implying that this mechanism is more effective in producing gravity changes when the mass source is located at shallow depths.

Progressive replacement of resident magma by magma having a different density is another mechanism that may lead to gravity changes not accompanied by the expected deformation. Bagnardi et al. (2014) suggested that sustained gas emission may lead to substitution of gas-rich magma in a bulk reservoir by outgassed magma sinking to deeper levels of the plumbing system. The resulting density increase within the reservoir induces a gravity change without any important volume change of the reservoir itself.

This mechanism could have acted during the first part of the 2009–2011 interval, when only sustained degassing occurred from the summit craters of Mt. Etna (Mattia et al. 2015), possibly leading to a densification of the inferred mass source at ~ 5 km b.s.l. Successively, when eruptive activity resumed from the summit craters, the recycling mechanism could have become progressively less efficient, eventually favouring the switch from density increase to decrease within the bulk reservoir.

Overall, gravity and vertical deformation data during 2009–2011 image a recharge phase, whereby most of the new material coming from below was stocked in the reservoir at intermediate depth through shrinking of the resident magma

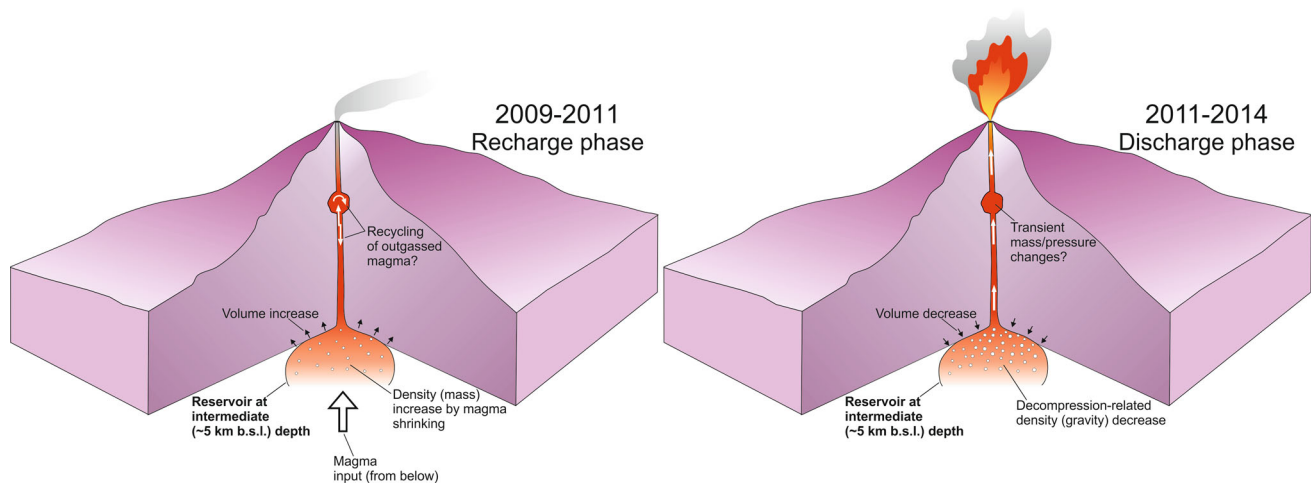


Fig. 9 Summary cartoon (not to scale) showing the inferred processes during 2009 to 2014. Left: during the 2009–2011 recharge phase, magma input from deep portions of the plumbing system caused pressure increase in a reservoir at about 5 km b.s.l. This led to bulk volume increase and density (mass) increase by magma compression. In turn, these processes caused the observed inflation and gravity increase. Right: since 2011, magma outflow from the reservoir at ~ 5 km depth towards shallower levels of the plumbing system progressively

exceeded the influx of magma from below. This led to the intense eruptive activity during 2011–2014 and the switch from pressure increase to decrease within the reservoir at ~ 5 km depth, which promoted bulk volume reduction, thus the observed subsidence, and decompression-related density decrease, observed at the surface as gravity decrease. Transient pressure and mass changes probably occurred in the shallower storage zone described by Bonforte et al. (2008) and Bonaccorso et al. (2011a), but over time-scales too short to be resolved by the gravity and GPS measurements in the focus of the present study

(left panel of Fig. 9). This view is supported by the findings of Paonita et al. (2016), who observed a marked increase in $^3\text{He}/^4\text{He}$ during early 2010 to early 2012. The latter was interpreted as due to a recharge event in a magma chamber at ~ 8 km depth. Recycling of outgassed, denser magma sinking from shallower levels, could have contributed to enhance the ratio of gravity change to vertical deformation during the 2009–2011 interval (left panel of Fig. 9).

Conversely, gravity decrease and subsidence during 2011 to 2014 are indicative of discharge from the reservoir at ~ 5 km b.s.l. (right panel of Fig. 9). We suppose that, during this interval, the influx of magma to the reservoir from below was much smaller than the outflow towards shallower levels of the plumbing system, which promoted bulk volume reduction (subsidence) and decompression-related (increase in the volume fraction of exsolved gas) density, thus gravity, decrease. The abrupt reduction in the $^3\text{He}/^4\text{He}$ signal during the first half of 2012 (Paonita et al. 2016) would suggest an overpressure decrease much faster than deduced from gravity and vertical deformation data (Fig. 4). This discrepancy could depend on the different depths of the storage regions imaged by the geochemical and geophysical data, where different, though related, processes could have taken place.

Within the limits of the available temporal resolution, the start of the gravity decrease and subsidence phase coincided with, or immediately followed, the resumption of sustained eruptive activity from the summit craters during the second half of 2011 (Fig. 4), when a sequence of closely spaced lava

fountains (5–10 days between successive events) occurred (Behncke et al. 2014). Until late 2014, ~ $150 \cdot 10^6 \text{ m}^3$ of material was emitted only through lava fountains from the NSEC (De Beni et al. 2015), which, taking into account that eruptive activity other than lava fountaining took place during the same interval, represents a minimum estimate of the total volume outputted by the volcano. Nevertheless, the above estimate, though lower, is still on the same order of magnitude as the volume deduced from inversion of the gravity decrease. These observations suggest that most magma inferred to have left the storage zone at ~ 5 km b.s.l., between 2011 and 2014, fed the eruptive activity from the summit craters of Mt. Etna during the same interval.

9 Concluding remarks

The availability of absolute gravity data from 11 points, at elevations of between 1150 and 2850 m on the slopes of Mt. Etna, allows to consistently track changes up to a few tens of μGals occurring over multi-year time scales, since 2009. That is not always possible with the more widely utilized relative (spring) gravimeters, since, in order to compare data acquired during different measurement campaigns, each campaign must be related to a reference outside the active area, assumed to be unaffected by volcano-related gravity changes (Carbone et al. 2017). Especially over long time scales (several months to years), this may introduce

significant errors, since possible variations at the reference station(s), due to man-made, hydrological, and other effects, will be propagated through the entire network. Furthermore, changes in the instrumental drift rate and tares (Rymer 1989) during a measurement campaign with a spring device will significantly increase the error budget.

The analysis of absolute gravity and ground elevation changes during 2009 to 2014 allows to recognize a long-term cycle of charge and discharge, occurring in a reservoir beneath the summit area of Mt. Etna, at depth of about 5 km b.s.l. (Fig. 9). In particular, the patterns of gravity and ground elevation changes indicate that, since 2009, thanks to the high (gas-enhanced) compressibility of the resident magma, this storage zone accommodated a large amount of new magma coming from deeper levels, before magma was transferred to shallower portions of the feeder system. Consideration of the eruptive activity during the studied period suggests that magma transfer to shallower levels started in early 2011, when the first episodes of lava fountaining in the 2011–2013 sequence occurred from the NSEC (Calvari et al. 2018). The emplacement of this upward mass transfer, likely associated with a reduced influx to the inferred storage zone at intermediate depth from below, progressively led to the switch from positive to negative gravity and ground elevation changes. Starting from the second half of 2011, when a cluster of closely-spaced lava fountains occurred (July to October 2011; Behncke et al. 2014), gravity decrease and subsidence (Fig. 5) indicate that the storage zone at 5 km b.s.l. was undergoing volume reduction and decompression-related density decrease (Fig. 9). This regime continued throughout the following ~ 2 years as the magma lost from the storage zone at intermediate depth fed the eruptive activity until late 2014.

Results of previous studies (Bonforte et al. 2008; Bonaccorso et al. 2011a) suggest that magma transfer from the storage at intermediate depth to a shallower part of the feeding system, located at about sea level, occurs prior to each Strombolian eruption or lava fountain event. Indeed, the shallow storage system is not able to accommodate large amounts of magma, implying that a tight overall balance between refilling and erupted magma is maintained (Bonaccorso et al. 2013; Bonforte et al. 2021). This view explains why long-term gravity and elevation changes are dominated by the effects of processes occurring in the storage zone at intermediate depth: possible effects linked to transitory disequilibrium in the shallower reservoir likely occur over time-scales too short to be resolved by the absolute gravity and GPS measurements in the focus of the present study.

We provide a further evidence of the great potential of joint gravity and ground deformation studies to enhance our understanding of how volcanoes work. Repeated absolute gravity measurements allowed to unambiguously track a long-term recharge phase, involving a much larger amount of magma

than one would have inferred from considering only the associated ground elevation changes. The accumulated magma fed volcanic activity during the subsequent ~ 2-year phase of discharge. Our results thus have important implications for the long-term volcanic hazard assessment and encourage the execution of absolute/hybrid gravity measurements (Greco et al. 2012) to complement ground deformation monitoring at volcanoes where bulk mass redistributions may develop over time scales of months to years.

Supplementary Information The online version contains supplementary material available at <https://doi.org/10.1007/s00190-022-01692-z>.

Acknowledgements Thanks are due to the UFDG staff of INGV-CT who carried out ground deformation measurements and helped to collect absolute and relative gravity data. We thank the AE and reviewers for their constructive suggestions, which greatly helped to improve our manuscript.

Author contributions FG designed the work, collected and analysed absolute gravity data and wrote the original draft paper. AB analysed GPS data and contributed to the editing of the manuscript. DC performed data modelling and contributed to the editing of the manuscript. All authors read and approved the final manuscript.

Funding This research was partially supported by the H2020 NEWTON-g project (Grant Agreement no. 801221).

Data availability The datasets used in this study are included in the article as supplementary files.

Declarations

Conflict of interest The authors declare that they have no competing interests.

Open Access This article is licensed under a Creative Commons Attribution 4.0 International License, which permits use, sharing, adaptation, distribution and reproduction in any medium or format, as long as you give appropriate credit to the original author(s) and the source, provide a link to the Creative Commons licence, and indicate if changes were made. The images or other third party material in this article are included in the article's Creative Commons licence, unless indicated otherwise in a credit line to the material. If material is not included in the article's Creative Commons licence and your intended use is not permitted by statutory regulation or exceeds the permitted use, you will need to obtain permission directly from the copyright holder. To view a copy of this licence, visit <http://creativecommons.org/licenses/by/4.0/>.

References

- Acocella V, Neri M, Behncke B, Bonforte A, Del Negro C, Ganci G (2016) Why does a mature volcano need new vents? The case of the new southeast crater at Etna. *Front Earth Sci*. <https://doi.org/10.3389/feart.2016.00067>
- Aloisi M, Jin S, Pulvirenti F, Scaltrito A (2017) The december 2015 Mount Etna eruption: an analysis of inflation/deflation phases and faulting processes. *J Geodynamics* 107:34–45. <https://doi.org/10.1016/j.jog.2017.03.003>

- Aloisi M, Bonaccorso A, Cannavò F, Currenti G (2018) Coupled short- and medium-term geophysical signals at Etna Volcano: using deformation and strain to infer magmatic processes from 2009 to 2017. *Front Earth Sci* 6:109. <https://doi.org/10.3389/feart.2018.00109>
- Alparone S, Barberi G, Bonforte A, Maiolino V, Ursino A (2011) Evidence of multiple strain fields beneath the eastern flank of Mt. Etna volcano (Sicily, Italy) deduced from seismic and geodetic data during 2003–2004. *Bull Volcanol* 73:869–885
- Alparone S, Bonaccorso A, Bonforte A, Currenti G (2013) Long-term stress-strain analysis of volcano flank instability: The eastern sector of Etna from 1980 to 2012. *J Geophys Res Solid Earth* 118:5098–5108
- Bagnardi M, Poland MP, Carbone D, Baker S, Battaglia M, Amelung F (2014) Gravity changes and deformation at Kīlauea Volcano, Hawaii, associated with summit eruptive activity, 2009–2012. *J Geophys Res* 119(9):7288–7305. <https://doi.org/10.1002/2014JB011506>
- Battaglia M, Hill DP (2009) Analytical modeling of gravity changes and crustal deformation at volcanoes: The Long Valley caldera, California, case study. *Tectonophysics* 471:45–57. <https://doi.org/10.1016/j.tecto.2008.09.040>
- Battaglia M, Segall P, Roberts CW (2003) The mechanics of unrest at Long Valley caldera, California. 2. Constraining the nature of the source using geodetic and micro-gravity data. *J Volcanol Geotherm Res* 127:219–245
- Battaglia M, Gottsmann J, Carbone D, Fernández J (2008) 4D volcano gravimetry. *Geophysics* 73(6):WA3–WA18. <https://doi.org/10.1190/1.2977792>
- Behncke B, Branca S, Corsaro RA, De Beni E, Miraglia L, Proietti C (2014) The 2011–2012 summit activity of Mount Etna: Birth, growth and products of the new SE crater. *J Volcanol Geotherm Res* 270:10–21
- Berrino G, Rymer H, Brown GC, Corrado G (1992) Gravity-height correlations for unrest at calderas. *J Volcanol Geotherm Res* 53:11–26. [https://doi.org/10.1016/0377-0273\(92\)90071-K](https://doi.org/10.1016/0377-0273(92)90071-K)
- Bonaccorso A, Calvari S (2017) A new approach to investigate an eruptive paroxysmal sequence using camera and strainmeter networks: lessons from the 3–5 December 2015 activity at Etna volcano. *Earth Planet Sci Lett* 475:231–241. <https://doi.org/10.1016/j.epsl.2017.07.020>
- Bonaccorso A, Bonforte A, Currenti G, Del Negro C, Di Stefano A, Greco F (2011a) Magma storage, eruptive activity and flank instability: Inferences from ground deformation and gravity changes during the 1993–2000 recharging of Mt. Etna volcano. *J Volcanol Geotherm Res* 200:245–254. <https://doi.org/10.1016/j.jvolgeores.2011.01.001>
- Bonaccorso A, Cannata A, Corsaro RA, Di Grazia G, Gambino S, Greco F, Miraglia L, Pistorio A (2011b) Multidisciplinary investigation on a lava fountain preceding a flank eruption: the 10 May 2008 Etna case. *Geochem Geophys Geosyst* 12:Q07009. <https://doi.org/10.1029/2010GC003480>
- Bonaccorso A, Caltabiano T, Currenti G, Del Negro C, Gambino S, Ganci G, Giammanco S, Greco F, Pistorio A, Salerno G, Spampinato S, Boschi E (2011c) Dynamics of a lava fountain revealed by geophysical, geochemical 2 and thermal satellite measurements: the case of the 10 April 2011 Mt. Etna eruption. *Geoph Res Lett.* <https://doi.org/10.1029/2011GL049637>
- Bonaccorso A, Currenti G, Linde A, Sacks S (2013) New data from borehole strainmeters to infer lava fountain sources (Etna 2011–2012). *Geophys Res Lett* 40:3579–3584. <https://doi.org/10.1002/grl.50692>
- Bonafede M, Ferrari C (2009) Analytical models of deformation and residual gravity changes due to a Mogi source in a viscoelastic medium. *Tectonophysics* 471:4–13
- Bonforte A, Guglielmino F (2008) Transpressive strain on the Lipari-Vulcano volcanic complex and dynamics of the “La Fossa” cone (Aeolian Islands, Sicily) revealed by GPS surveys on a dense network. *Tectonophysics* 457:64–70. <https://doi.org/10.1016/j.tecto.2008.05.016>
- Bonforte A, Guglielmino F (2015) Very shallow dyke intrusion and potential slope failure imaged by ground deformation: the 28 December 2014 eruption on Mount Etna. *Geophys Res Lett* 42:2727–2733. <https://doi.org/10.1002/2015GL063462>
- Bonforte A, Puglisi G (2006) Dynamics of the eastern flank of Mt. Etna volcano (Italy) investigated by a dense GPS network. *J Volcanol Geotherm Res* 153:357–369. <https://doi.org/10.1016/j.jvolgeores.2005.12.005>
- Bonforte A, Carbone D, Greco F, Palano M (2007) Intrusive mechanism of the 2002 NE-rift eruption at Mt Etna (Italy) modelled using GPS and gravity data. *Geophys J Int* 169:339–347. <https://doi.org/10.1111/j.1365-246X.2006.03249.x>
- Bonforte A, Bonaccorso A, Guglielmino F, Palano M, Puglisi G (2008) Feeding system and magma storage beneath Mt. Etna as revealed by recent inflation/deflation cycles. *J Geophys Res* 113:B05406. <https://doi.org/10.1029/2007JB005334>
- Bonforte A, Guglielmino F, Coltelli M, Ferretti A, Puglisi G (2011) Structural assessment of Mount Etna volcano from Permanent Scatterers analysis. *Geochem Geophys Geosyst* 12:Q02002. <https://doi.org/10.1029/2010GC003213>
- Bonforte A, Guglielmino F, Puglisi G (2013) Interaction between magma intrusion and flank dynamics at Mt. Etna in 2008, imaged by integrated dense GPS and DInSAR data. *Geochem Geophys Geosys* 14:2818–2835. <https://doi.org/10.1002/ggge.20190>
- Bonforte A, Fagone S, Giardina C, Genovese S, Aiesi G, Calvagna F, Cantarero M, Consoli O, Consoli S, Guglielmino F, Puglisi B, Puglisi G, Saraceno B (2016) Global positioning system survey data for active seismic and volcanic areas of eastern Sicily, 1994 to 2013. *Sci Data* 3:160062. <https://doi.org/10.1038/sdata.2016.62>
- Bonforte A, Fanizza G, Greco F, Matera A, Sulpizio R (2017) Long-term dynamics across a volcanic rift: 21 years of microgravity and GPS observations on the southern flank of Mt. Etna Volcano. *J Volcanol Geotherm Res.* <https://doi.org/10.1016/j.jvolgeores.2017.06.005>
- Bonforte A, Cannavò F, Gambino S, Guglielmino F (2021) Combining high- and low-rate geodetic data analysis for unveiling rapid magma transfer feeding a sequence of violent summit paroxysms at Etna in late 2015. *Appl Sci* 11:4630. <https://doi.org/10.3390/app11104630>
- Bonvalot S, Remy D, Deplus C, Diament M, Gabalda G (2008) Insights on the March 1998 eruption at Piton de la Fournaise volcano (La Réunion) from microgravity monitoring. *J Geophys Res.* <https://doi.org/10.1029/2007JB005084>
- Bruno V, Mattia M, Aloisi M, Palano M, Cannavò F, Holt WE (2012) Ground deformations and volcanic processes as imaged by CGPS data at Mt. Etna (Italy) between 2003 and 2008. *J Geophys Res* 117:B07208. <https://doi.org/10.1029/2011JB009114>
- Bruno V, Ferlito C, Mattia M, Monaco C, Rossi M, Scandura D (2016) Evidence of a shallow magma intrusion beneath the NE Rift system of Mt. Etna during 2013. *Terra Nova* 28:356–363. <https://doi.org/10.1111/ter.12228>
- Budetta G, Carbone D (1998) Temporal variations in gravity at Mt Etna (Italy) associated with the 1989 and 1991 eruptions. *Bull Volcanol* 59:311–326
- Budetta G, Grimaldi M, Luongo G (1989) Variazioni di gravità nell’area etnea (1986–1989). *Boll GNV* 5:137–146
- Budetta G, Carbone D, Greco F (1999) Subsurface mass redistribution at Mount Etna (Italy) during the 1995–1996 explosive activity detected by microgravity studies. *Geophys J Int* 138(1):77–88. <https://doi.org/10.1046/j.1365-246x.1999.00836.x>
- Calvari S, Cannavò F, Bonaccorso A, Spampinato L, Pellegrino AG (2018) Paroxysmal explosions, lava fountains and ash plumes at

- Etna Volcano: Eruptive processes and hazard implications. *Front Earth Sci* 6:107. <https://doi.org/10.3389/feart.2018.00107>
- Cannata A, Spedalieri G, Behncke B, Cannavò F, Di Grazia G, Gambino S, Gresta S, Gurrieri S, Liuzzo M, Palano M (2015) Pressurization and depressurization phases inside the plumbing system of Mount Etna volcano: Evidence from a multiparametric approach. *J Geophys Res Solid Earth* 120:5965–5982. <https://doi.org/10.1002/2015JB012227>
- Carbone D, Greco F (2007) Review of microgravity observations at Mt. Etna: a powerful tool to monitor and study active Volcanoes. *Pure Appl Geophys* 164:769–790. <https://doi.org/10.1007/s00024-007-0194-7>
- Carbone D, Budetta G, Greco F (2003) Possible mechanisms of magma redistribution under Mt. Etna during the 1994–1999 period detected through microgravity measurements. *Geophys J Int* 153(1):187–200. <https://doi.org/10.1046/j.1365-246X.2003.01901.x>
- Carbone D, Currenti G, Del Negro C (2008) Multiobjective genetic algorithm inversion of ground deformation and gravity changes spanning the 1981 eruption of Etna Volcano. *J Geophys Res.* <https://doi.org/10.1029/2006JB004917>
- Carbone D, D'Amico S, Musumeci C, Greco F (2009) Comparison between the 1994–2006 seismic and gravity data from Mt. Etna: new insight into the long-term behaviour of a complex volcano. *Earth Planet Sci Lett.* <https://doi.org/10.1016/j.epsl.2009.01.007>
- Carbone D, Aloisi M, Vinciguerra S, Puglisi G (2014) Stress, strain and mass changes at Mt. Etna during the period between the 1991–1993 and 2001 flank eruptions. *Earth-Sci Rev.* <https://doi.org/10.1016/j.earscirev.2014.07.004>
- Carbone D, Zuccarello L, Messina A, Scollo S, Rymer H (2015) Balancing bulk gas accumulation and gas output before and during lava fountaining episodes at Mt. Etna. *Sci Rep.* <https://doi.org/10.1038/srep1804>
- Carbone D, Poland MP, Diamant M, Greco F (2017) The added value of time-variable microgravimetry to the understanding of how volcanoes work. *Earth Sci Rev* 169:146–179. <https://doi.org/10.1016/j.earscirev.2017.04.014>
- Currenti G (2014) Numerical evidences enabling to reconcile gravity and height changes in volcanic areas. *Geophys J Int* 197(1):164–173. <https://doi.org/10.1093/gji/ggt507>
- D'Agostino G, Desogus S, Germak A, Origlia C, Quagliotti D, Berrino G, Corrado G, Ricciardi G (2008) The new IMG-C-02 transportable absolute gravimeter: measurement apparatus and applications in geophysics and volcanology. *Ann Geophys* 51(1):39–49
- De Beni E, Behncke B, Branca S, Nicolosi I, Carluccio R, D'Ajello Caracciolo F et al (2015) The continuing story of Etna's New Southeast Crater (2012–2014): evolution and volume calculations based on field surveys and aerophotogrammetry. *J Volcanol Geotherm Res* 303:175–186. <https://doi.org/10.1016/j.jvolgeores.2015.07.021>
- de Zeeuw-van DE, Rymer H, Sigmundsson F, Sturkell E (2005) Net gravity decrease at Askja volcano, Iceland: constraints on processes responsible for continuous caldera deflation, 1988–2003. *J Volcanol Geotherm Res* 139(3–4):227–239. <https://doi.org/10.1016/j.jvolgeores.2004.08.008>
- de Zeeuw-van Dalfsen E, Rymer H, Williams-Jones G, Sturkell E, Sigmundsson F (2006) Integration of micro-gravity and geodetic data to constrain shallow system mass changes at Krafla volcano, N Iceland. *Bull Volcanol* 68(5):420–431. <https://doi.org/10.1007/s0445-005-0018-5>
- Del Negro C, Currenti G, Solaro G, Greco F, Pepe A, Napoli R, Pepe S, Casu F, Sansosti E (2013) Capturing the fingerprint of Etna volcano activity in gravity and satellite radar data. *Sci Rep* 3:3089. <https://doi.org/10.1038/srep03089>
- Falk R, Pálinská V, Wziontek H, Rülke A, Vaňko M, Ullrich C, Butta H, Kostelecký J, Bilker-Koivula M, Näränen J, Prato A, Mazzoleni F, Kırbaç C, Coşkun I, Van Camp M, Castelein S, Bernard JD, Lothhammer A, Schilling M, Timmen L, Iacovone D, Nettis G, Greco F, Messina A, Reudink R, Petrini M, Dykowski P, Sękowski M, Janák J, Papco J, Engfeldt A, Steffen H (2020) Final report of EURAMET.M.G-K3 regional comparison of absolute gravimeters. *Metrologia.* <https://doi.org/10.1088/0026-1394/57/1a/07019>
- Greco F, Currenti G, Del Negro C, Napoli R, Budetta G, Fedi M, Boschi E (2010) Spatio-temporal gravity variations to look deep into the southern flank of Etna volcano. *J Geophys Res* 115(B):11411. <https://doi.org/10.1029/2009JB006835>
- Greco F, Currenti G, D'Agostino G, Germak A, Napoli R, Pistorio A, Del Negro C (2012) Combining relative and absolute gravity measurements to enhance volcano monitoring at Mt. Etna (Italy). *Bull Volcanol.* <https://doi.org/10.1007/s00445-012-0630-0>
- Greco F, Iafolla V, Pistorio A, Fiorenza E, Currenti G, Napoli R, Bonaccorso A, Del Negro C (2014) Characterization of the response of spring-based relative gravimeters during paroxysmal eruptions at Etna volcano. *Earth Planets Space.* <https://doi.org/10.1186/1880-5981-66-44>
- Greco F, Biolcati E, Pistorio A, D'Agostino G, Germak A, Origlia C, Del Negro C (2015) Absolute gravity measurements at three sites characterized by different environmental conditions using two portable ballistic gravimeters. *Eur Phys J plus* 130:38. <https://doi.org/10.1140/epjp/i2015-15038-0>
- Greco F, Currenti G, Palano M, Pepe A, Pepe S (2016) Evidence of a shallow persistent magmatic reservoir from joint inversion of gravity and ground deformation data: the 25–26 October 2013 Etna lava fountaining event. *Geophys Res Lett.* <https://doi.org/10.1002/2016GL068426>
- Hajian A, Cannavò F, Greco F, Nunnari G (2019) Classification of Mount Etna (Italy) Volcanic Activity by Machine Learning Approaches. *Ann Geophys.* <https://doi.org/10.4401/ag-8049>
- Jiang Z, Palinkas V, Arias FE, Liard J, Merlet S, Wilmes H, Vitushkin L, Robertsson L, Tisserand L, Pereira Dos Santos F, Bodart Q, Falk R, Baumann H, Mizushima S, Makinen J, Bilker-Koivula M, Lee C, Choi IM, Karaboce B, Ji W, Wu Q, Ruess D, Ullrich C, Kostelecký J, Schmerge D, Eckl M, Timmen L, Le Moigne N, Bayer R, Olszak T, Agren J, Del Negro C, Greco F, Diamant M, Deroussi S, Bonvalot S, Krynski J, Sekowski M, Hu H, Wang LJ, Svitlov S, Germak A, Francis O, Becker M, Inglis D, Robinson I (2012) The 8th International Comparison of Absolute Gravimeters 2009: the first Key Comparison (CCM.G-K1) in the field of absolute gravimetry. *Metrologia* 49:666–684. <https://doi.org/10.1088/0026-1394/49/6/666>
- Johnson DJ, Eggers AA, Bagnardi M, Battaglia M, Poland MP, Miklius A (2010) Shallow magma accumulation at Kīlauea Volcano, Hawai'i, revealed by microgravity surveys. *Geology* 38(12):1139–1142. <https://doi.org/10.1130/G31323.1>
- Kilbride B, Edmonds M, Biggs J (2016) Observing eruptions of gas-rich compressible magmas from space. *Nat Commun* 7:13744. <https://doi.org/10.1038/ncomms13744>
- Mattia M, Bruno V, Caltabiano T, Cannata A, Cannavò F, D'Alessandro W, Liuzzo M (2015) A comprehensive interpretative model of slow slip events on Mt. Etna's Eastern Flank. *Geochem Geophys Geosyst* 16:635–658. <https://doi.org/10.1002/2014GC005585>
- McTigue DF (1987) Elastic stress and deformation near a finite spherical magma body: resolution of the point source paradox. *J Geophys Res Solid Earth.* <https://doi.org/10.1029/JB092iB12p12931>
- Merriam JB (1992) Atmospheric pressure and gravity. *Geophys J Int* 109(3):488–500. <https://doi.org/10.1111/j.1365-246X.1992.tb00112.x>
- Moretti R, Métrich N, Arienzo I, Di Renzo V, Aiuppa A, Allard P (2018) Degassing vs. eruptive styles at Mt. Etna volcano (Sicily, Italy). Part I: volatile stocking, gas fluxing, and the shift from low-energy to highly explosive basaltic eruptions. *Chem Geol* 482:1–17. <https://doi.org/10.1016/j.chemgeo.2017.09.017>

- Napoli R, Currenti G, Del Negro C, Greco F, Scandura D (2008) Volcanomagnetic evidence of the magmatic intrusion on 13th May 2008 Etna eruption. *Geoph Res Lett* 35:L22301. <https://doi.org/10.1029/2008GL035350>
- Newell DB, Westrum D Van, Francis O, Kanney J, Liard J, Ramirez AE, Lucero B, Ellis B, Greco F, Pistorio A, Reudink R, Iacovone D, Baccaro F, Silliker J, Wheeler RD, Falk R, Ruelke A (2017) Regional comparison of absolute gravimeters SIM.M.G-K1 key comparison. *Metrologia* 54(1A):07019 - Technical Supplement. doi: <https://doi.org/10.1088/0026-1394/54/1A/07019>
- Niebauer TM, Sasagawa GS, Faller JE, Hilt R, Klopping F (1995) A new generation of absolute gravimeters. *Metrologia* 32(3):159–180. <https://doi.org/10.1088/0026-1394/32/3/004>
- Obrizzo F, Pingue F, Troise C, De Natale G (2004) Bayesian inversion of 1994–1998 vertical displacements at Mt Etna: evidence for magma intrusion. *Geophys J Int.* <https://doi.org/10.1111/j.1365-246X.2004.0210.x>
- Pálinkáš V, Francis O, Val'ko M, Kostelecký J, Camp M Van, Castelein S, Bilker-Koivula M, Näränen J, Lothhammer A, Falk R, Schilling M, Timmen L, Iacovone D, Baccaro F, Germak A, Biolcati E, Origlia C, Greco F, Pistorio A, De Plaen R, Klein G, Seil M, Radinovic R, Reudink R, Dykowski P, Sękowski M, Próchniewicz D, Szpunar R, Mojzeš M, Jaňk J, Papčo J, Engfeldt A, Olsson PA, Smith V, Westrum D Van, Ellis B, Lucero B (2017) Regional comparison of absolute gravimeters, EURAMET.M.G-K2 key comparison. *Metrologia* 54(1A):07012 - Technical Supplement. <https://doi.org/10.1088/0026-1394/54/1A/07012>
- Paonita A, Caracausi A, Martelli M, Rizzo A (2016) Temporal variations of helium isotopes in volcanic gases quantify pre-eruptive refill and pressurization in magma reservoirs: the Mount Etna case. *Geol (geol Soc Am)*. <https://doi.org/10.1130/G37807.1>
- Petit G, Luzum B IERS Conventions (2010) IERS Technical Note 36, Frankfurt am Main: Verlag des Bundesamts für Kartographie und Geodäsie, 2010
- Pistorio A, Greco F, Currenti G, Napoli R, Sicali A, Del Negro C, Fortuna L (2011) High precision gravity measurements using absolute and relative gravimeters at Mount Etna (Sicily, Italy). *Ann Geophys* 54:5. <https://doi.org/10.4401/ag-5348>
- Puglisi G, Briole P, Bonforte A (2004) Twelve years of ground deformation studies on Mt Etna volcano based on GPS surveys. In: Bonaccorso A, Calvari S, Coltelli M, Del Negro C, Falsaperla S (eds) Mt. Etna: Volcano laboratory. AGU Geophys. Monograph Series, vol 143. AGU, Washington, pp 321–341
- Rivalta E, Segall P (2008) Magma compressibility and the missing source for some dike intrusions. *Geoph Res Lett* 35:L04306. <https://doi.org/10.1029/2007GL032521>
- Rymer H (1989) A contribution to precision microgravity data analysis using Lacoste and Romberg gravity meters. *Geophys J* 97(31):1–322
- Rymer H, Murray JB, Brown GC, Ferrucci F, McGuire WJ (1993) Mechanisms of magma eruption and emplacement at Mt. Etna between 1989 and 1992. *Nature* 361(6411):439–441. <https://doi.org/10.1038/361439a0>
- Slatcher N, James MR, Calvari S, Ganci G, Browning J (2015) Quantifying effusion rates at active volcanoes through integrated timelapse laser scanning and photography. *Remote Sens* 7:14967–14987. <https://doi.org/10.3390/rs71114967>
- Spampinato L, Sciotto M, Cannata A, Cannavò F, La Spina A, Palano M et al (2015) Multiparametric study of the February–April 2013 paroxysmal phase of Mt. Etna New South-East crater. *Geochem Geophys Geosyst* 16:1932–1949. <https://doi.org/10.1002/2015GC005795>
- Timmen L (2003) Precise definition of the effective measurement height of free-fall absolute gravimeters. *Metrologia* 40(2):62. <https://doi.org/10.1088/0026-1394/40/2/310>
- Urlaub M, Petersen F, Gross F, Bonforte A, Puglisi G, Guglielmino F, Krastel S, Lange D, Kopp H (2018) Gravitational collapse of Mount Etna's southeastern flank. *Sci Adv* 4(10):eaat9700. <https://doi.org/10.1126/sciadv.aat9700>
- Vulpiani G, Ripepe M, Valade S (2016) Mass discharge rate retrieval combining weather radar and thermal camera observations. *J Geophys Res Solid Earth* 121:5679–5695. <https://doi.org/10.1002/2016JB013191>